AGU PUBLICATIONS

JGR

Journal of Geophysical Research: Space Physics

RESEARCH ARTICLE
10.1002/2016JA023648

Key Points:
- Low-energy electrons (tens to hundreds of eV) originate from two main sources: the ionosphere and the plasma sheet
- Low-energy electrons pervade the inner magnetosphere where they can drive wave-particle interactions
- Fluxes of electrons from ~30 eV to 1 keV are quantified by pitch-angle, L value, and local time for both quiet and active periods

Correspondence to:
M. H. Denton,
mdenton@spacescience.org

Citation:
Denton, M. H., G. D. Reeves, B. A. Larsen, R. F. W. Friedel, M. F. Thomsen, P. A. Fernandes, R. M. Skoug, H. O. Funsten, and L. K. Sarno-Smith (2017), On the origin of low-energy electrons in the inner magnetosphere: Fluxes and pitch-angle distributions, *J. Geophys. Res. Space Physics*, *122*, 1789–1802, doi:10.1002/2016JA023648.

Received 4 NOV 2016
Accepted 26 JAN 2017
Accepted article online 31 JAN 2017
Published online 15 FEB 2017

On the origin of low-energy electrons in the inner magnetosphere: Fluxes and pitch-angle distributions

M. H. Denton[1,2], G. D. Reeves[1,3], B. A. Larsen[1,3], R. F. W. Friedel[1,3], M. F. Thomsen[4], P. A. Fernandes[3], R. M. Skoug[3], H. O. Funsten[3], and L. K. Sarno-Smith[5]

[1]New Mexico Consortium, Los Alamos, New Mexico, USA, [2]Center for Space Plasma Physics, Space Science Institute, Boulder, Colorado, USA, [3]Los Alamos National Laboratory, Los Alamos, New Mexico, USA, [4]Planetary Science Institute, Tucson, Arizona, USA, [5]Department of Climate and Space Sciences and Engineering, University of Michigan, Ann Arbor, Michigan, USA

Abstract Accurate knowledge of the plasma fluxes in the inner magnetosphere is essential for both scientific and programmatic applications. Knowledge of the low-energy electrons (approximately tens to hundreds of eV) in the inner magnetosphere is particularly important since these electrons are acted upon by various physical processes, accelerating the electrons to higher energies, and also causing their loss. However, measurements of low-energy electrons are challenging, and as a result, this population has been somewhat neglected previously. This study concerns observations of low-energy electrons made by the Helium Oxygen Proton Electron instrument on board the Van Allen Probes satellites and also observations from geosynchronous orbit made by the Magnetospheric Plasma Analyzer on board Los Alamos National Laboratory satellites. The fluxes of electrons from ~30 eV to 1 keV are quantified as a function of pitch-angle, McIlwain L parameter, and local time for both quiet and active periods. Results indicate two sources for low-energy electrons in this energy range: the low-energy tail of the electron plasma sheet and the high-energy tail of the dayside ionosphere. These populations are identified primarily as a result of their different pitch-angle distributions. Field-aligned outflows from the dayside ionosphere are observed at all L shells during quiet and active periods. Our results also demonstrate that the dayside electron field-aligned fluxes at ~30 eV are particularly strong between L values of 6 and 7, indicating an enhanced source within the polar ionosphere.

1. Introduction

Measurements of the low-energy (tens to hundreds of eV) electron population in the inner magnetosphere are challenging. This is largely due to the combined effects of (i) surface charging that results in a net charge on orbiting satellites [*DeForest*, 1972; *Garrett*, 1981; *Farthing et al.*, 1982; *Lanzerotti et al.*, 1998; *Thomsen et al.*, 2013], (ii) photoelectrons and secondary electrons that may be trapped in potential wells around the satellite, and (iii) the effects of penetrating radiation that can obscure observations of low-energy particles. In the inner magnetosphere all of these issues make it difficult to determine the "real" electron population. For a negatively charged spacecraft, ambient electrons that have energies below the surface potential of the spacecraft are not detected since they are repelled from the onboard detection instrumentation. Conversely, electrons that are detected may be from photoelectrons, secondary electrons, electrons accelerated toward the satellite due to a positive spacecraft potential, or from false counts due to penetrating radiation. Distinguishing the ambient electron population from these combined effects is not trivial.

As a result of these issues, the dynamics and evolution of the low-energy electron population in the energy range of tens to hundreds of eV have been somewhat neglected in comparison with other magnetospheric populations such as the bulk plasmasphere, the plasma sheet, and the radiation belts. The situation is analogous to, and may be compared directly with, the study of low-energy ions in the magnetosphere—previously termed the "hidden ion population of the magnetosphere" [*Olsen*, 1982; *Olsen et al.*, 1985]. This low-energy ion population (that is also challenging to measure due to charging issues) has recently received renewed attention and, as a result, a better appreciation of its role in global magnetospheric dynamics [*Chappell et al.*, 2008; *Sarno-Smith et al.*, 2015; *Denton et al.*, 2016b]. It is hoped that the work in this current paper contributes to a similar advancement in understanding the low-energy electron population. Low-energy electrons are of particular importance to magnetospheric system dynamics due to their role in modulation of

wave-growth in particular and wave-particle interactions in general [*Thorne and Horne*, 1994; *Bell et al.*, 2002; *Bortnik et al.*, 2007; *Li et al.*, 2010].

Outflow from the sunlit low-latitude ionosphere results in the formation of the plasmasphere, a mixture of electrons and ions with a characteristic energy of ~1 eV, that exists on corotating magnetic field lines [*Storey*, 1953; *Gringauz et al.*, 1960; *Carpenter*, 1963; *Chappell et al.*, 1971; *Chappell*, 1972, *Carpenter and Park*, 1973; *Chappell et al.*, 2008]. In contrast, the auroral ionosphere is heavily influenced by particle precipitation in addition to solar EUV. This results in additional outflow (and energization) of electrons and ions onto convecting magnetic field lines, both on the dayside and the nightside; energies from a few tens of eV are typical for electrons, although the most energetic electrons may reach low keV energies [*Johnstone and Winningham*, 1982; *Teste et al.*, 2007]. It has been shown that downward currents are carried by the field-aligned electrons [*Klumpar and Heikkila*, 1982], and on the nightside, outflowing electrons provide one important source of material for the tail plasma sheet. The other source for the plasma sheet is the entry of ions and electrons into the magnetosphere from the solar wind. A range of studies have previously reported electrons in the magnetotail with energies of approximately tens to hundreds of eV [e.g., *Christon et al.*, 1991; *Zwolakowska et al.*, 1992]. The electrons (and ions) that form the nightside plasma sheet are delivered into the inner magnetosphere by magnetospheric convection, and energies around 1 keV are common at geosynchronous orbit (GEO) [*Thomsen et al.*, 1998a; *Korth et al.*, 1999; *Friedel et al.*, 2001; *Denton et al.*, 2005; *Lavraud et al.*, 2005; *Henderson et al.*, 2015; *Denton et al.*, 2016a]. Such observations are consistent with the adiabatic energization of a lower energy population of electrons that is convected Earthward.

Hence, there are (at least) two sources for electrons with energies approximately tens to hundreds of eV. First, the high-energy tail of the thermal ionospheric population (cf. *Klumpar and Heikkila*, 1982; *Li et al.*, 2010; *Denton and Borovsky*, 2014), and second, the low-energy tail of the warm plasma sheet population [cf. *Christon et al.*, 1991; *Denton et al.*, 2005, 2015]. Recent work by *Li et al.* [2010] has demonstrated that electrons with energies ~100 eV pervade the magnetosphere and are found both inside and outside the plasmasphere. It should also be noted that, when discussing the spectral characteristics of the electron population in the central plasma sheet, *Christon et al.* [1991] found that the ratio of the cold population (energies from ~30 eV to ~1 keV) to the warm component (energies greater than ~1 keV) was ~0.4 (in terms of electron number density). In 12% of cases they studied, the cold electron density was more than twice the density of the warmer components. Clearly, the lower energy electron population has the potential to play an important role in the magnetosphere and there is a need to better understand its morphology and dynamics.

The ultimate aim of this study is to document the characteristics of the low-energy electron population in the magnetosphere under a range of different conditions. In addition, we hope to shed light on the origins of this population. The potential importance of low-energy electrons within the larger complex and coupled magnetospheric system is emphasized [cf. *Denton et al.*, 2016b]. Since the system exhibits nonlinear effects such as feedback and time-lag dependencies, it is essential to have physical knowledge (and understanding) of all system components in order to fully understand the global system dynamics. We use data from the NASA Van Allen Probes (formerly Radiation Belt Storm Probes) mission [*Mauk et al.*, 2013] and from the Los Alamos National Laboratory (LANL) satellites in geosynchronous orbit [*Bame et al.*, 1993] to explore the spatial and pitch-angle distributions of electrons between L = 2 and L = 6.6. Our analysis is concentrated on electrons with characteristic energies from ~30 eV to ~1 keV, although the populations both below and above these energies are also discussed.

2. Data Analysis

The main data set used in the analysis originates from electron measurements made by the Helium Oxygen Proton Electron (HOPE) plasma spectrometer [*Funsten et al.*, 2013; *Spence et al.*, 2013] on board the Van Allen Probes satellites. HOPE is a spherical electrostatic analyzer that measures the electron distribution between ~1 eV and 50 keV.

Since the analysis in this paper is specifically aimed at low-energy electrons, it is critical that surface charging on the spacecraft is low, that the effects from photoelectrons and secondaries are minimized, and that penetrating background radiation is mostly negligible, in order that the instrumentation reports fluxes based on the conditions in orbit. A large effort was made in the design of the satellite

platform and in the choice of materials used in construction, in order to minimize the buildup of surface charge on the spacecraft, to prevent localized potential wells, and to inhibit the effects of penetrating background radiation [*Kirby et al.*, 2013]. This effort was supplemented by prelaunch environmental tests that demonstrated that the platform would have a very low susceptibility to surface charging once on orbit [*Kirby et al.*, 2013]. The level of spacecraft charging can be estimated from the Electric Fields and Waves (EFW) instrument on board Van Allen Probes [*Wygant et al.*, 2013]. A recent study of spacecraft potential on Van Allen Probes by using data from February 2013 to April 2015 revealed that, during the vast majority of the mission, the platform charged to a slightly positive level between 0 and 10 V. The instances where the satellite charged to a potential below −50 V were ≪1% of the total [*Sarno-Smith et al.*, 2016]. Hence, given the statistical nature of this study, times when spacecraft charging will *statistically* affect the HOPE electron observations (where millions of points are considered) are negligible. However, to exclude these instances from the analysis, we use the charging data from the *Sarno-Smith et al.* [2016] study (a combination of ion-line observations from HOPE and observations from the Electric Fields and Waves (EFW) instrument [*Wygant et al.*, 2013])—all data where satellite potential falls below −30 V are omitted.

In the current study all available pitch-angle-resolved electron observations made by Van Allen Probes B, from 13 October 2012 to 7 April 2015, are utilized for statistical analysis. Since the energies of the 72 channels on the HOPE instrument are not fixed, initially, all data are assigned to a grid that is fixed in energy with 72 energy bins, each evenly spaced (logarithmically) in energy, from 1 eV to 79 keV [cf. *Denton et al.*, 2016b]. This energy coverage spans the entire range (and beyond) of the HOPE instrument.

3. Results and Discussion

Figure 1 contains plots of the probability distribution of the omnidirectional electron flux measured by Van Allen Probes B at six energies (~33, 53, 118, 222, 576, and 1087 eV) and all L values, between October 2012 and May 2016. In general, the occurrence at each energy is peaked at a particular value of the flux, with higher fluxes more likely at lower energies. However, it is also evident that the probability distributions are not normally distributed. There is evidence (e.g., the "shoulder" to the right of the peak flux) that these distributions are superpositions of (at least) two distinct electron populations.

Figure 2 shows a more complete picture of the omnidirectional electron flux at two energies (32.98 eV and 1087 eV) as a function of magnetic local time (MLT) and the McIlwain L parameter. Each individual data point measured between October 2012 and May 2016 binned into a grid of 24 local time bins (1 h width) and 24 bins in L value (0.25 width). The flux at 1087 eV (Figure 2, top) is well-ordered with the highest flux values evident at L values greater than ~4, predominantly on the nightside. The flux at 32.98 eV (Figure 2, bottom) is also well-ordered with higher fluxes evident both at L values less than ~2.5, mostly on the dayside, and at L values greater than ~4.5, also on the nightside. It should be noted that, upon investigation, at both energies, there appear to be occasionally fluxes between L values of 1 and 2 at all local times. The investigation reveals that, although HOPE is designed to be largely insensitive to penetrating background fluxes, at these altitudes, highly energetic particles (likely relativistic protons) are penetrating the HOPE instrument and causing false electron counts. For the statistical results shown in Figure 2 the effect of the penetrating background is just evident between L ~ 1.25 and 1.50 at 1087 eV. At 32.98 eV the increased fluxes due to background are negligible compared to the ambient flux, on both dayside and nightside.

In order to provide comparisons with independent electron observations, at greater distances from the Earth than those sampled by NASA/Van Allen Probes, the HOPE data are supplemented by electron measurements from Magnetospheric Plasma Analyzer (MPA) instruments on seven Los Alamos National Laboratory (LANL) satellites in geosynchronous orbit (GEO). The complete LANL/MPA data set spans over two full solar cycles (1989 to Present). Here the analysis is based on data taken between 1989 and 2007. A full description of the LANL/MPA instrument can be found in *Bame et al.* [1993], with a detailed discussion of the individual spacecraft detector efficiencies, corrections for spacecraft surface charging, instrument background estimations, etc., presented by *Thomsen et al.* [1999].

Previous investigation of the averaged electron (and ion) fluxes at GEO, derived from the LANL/MPA data set, may be found in *Thomsen et al.* [2007]. In that study the electron and ion fluxes, over more than a full solar cycle, were averaged in order to determine the variability of fluxes as a function of activity, solar cycle, etc.

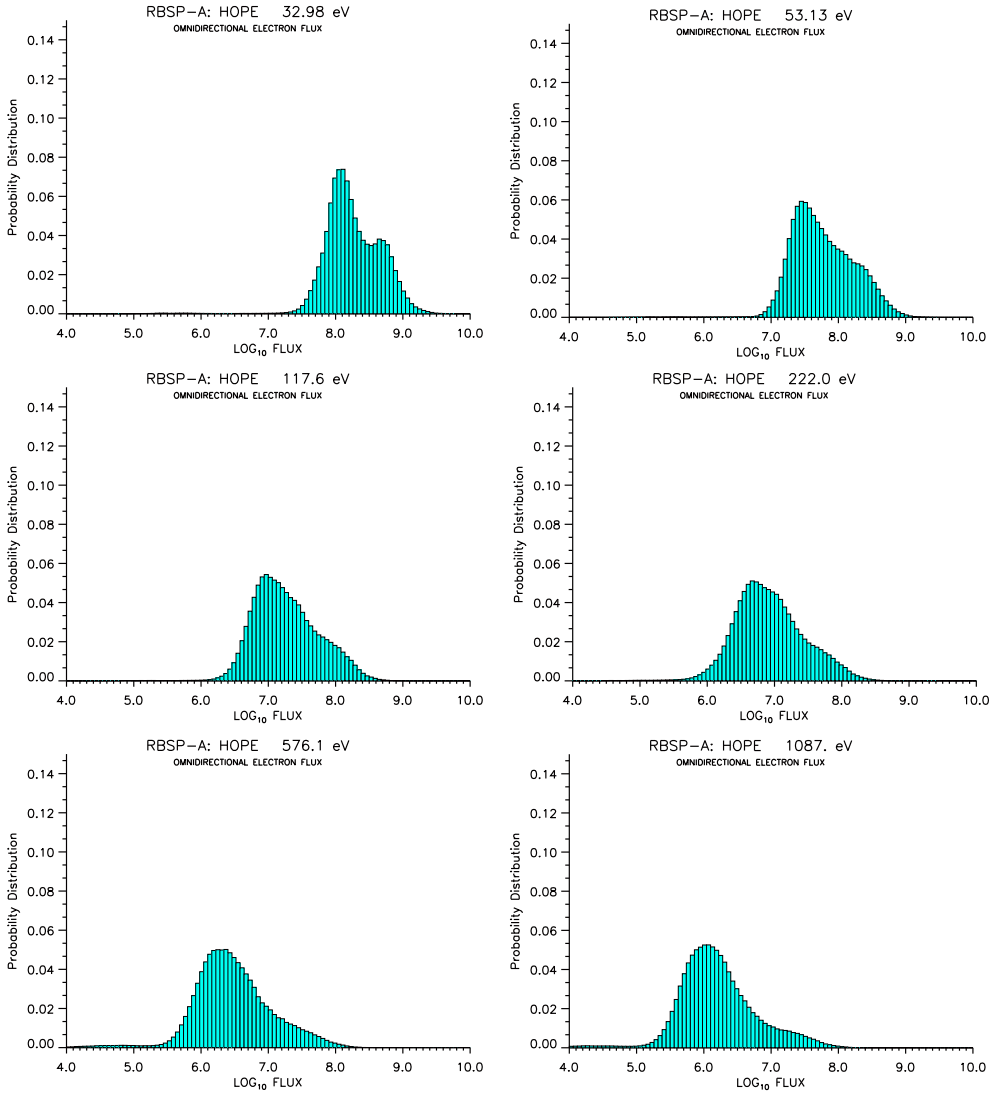

Figure 1. The probability distributions of the omnidirectional electron flux ($s^{-1}\,cm^{-2}\,sr^{-1}\,keV^{-1}$) at six energies from ~30 eV to ~1 keV based on all Radiation Belt Storm Probes (RBSP) A fluxes between October 2012 and May 2016. The distribution at each energy shows evidence that the distributions are composed of a superposition of more than one single electron population.

Figure 3 contains plots of the averaged flux measured by LANL/MPA, as a function of *Kp* and local time, at four energies (~64 eV, ~110 eV, ~540 eV, and ~1220 eV). The *Kp* index is used since it has previously been demonstrated to be a good proxy for the level of magnetospheric convection [*Thomsen*, 2004] and provides a good description of the access of plasma sheet plasma to GEO [*Korth et al.*, 1999; *Friedel et al.*, 2001]. Intervals where the magnetopause was located inward of GEO are excluded from the current analysis [cf. *Denton et al.*, 2005; *Denton and Borovsky*, 2013].

The average spacecraft charging levels for the LANL/MPA satellites as a function of *Kp*, *Dst*, solar wind velocity, and local time have been documented by *Denton and Borovsky* [2012], and *Denton et al.* [2016a]. In addition, an extensive analysis of surface charging on the LANL satellites and its relationship with electron temperature can be found in *Thomsen et al.* [2013]. Two points are worthy of note. In times of eclipse the surface charge on the LANL satellites can drop below −1000 V, although this is routinely corrected for in the analysis code and flux determination [*Thomsen et al.*, 1999]. Here to be as certain as possible that charging-related effects are minimized, we restrict our analysis to intervals where the level of spacecraft surface charging is low (>−40 V) and thus to intervals when the effects of secondary electrons will be minimized

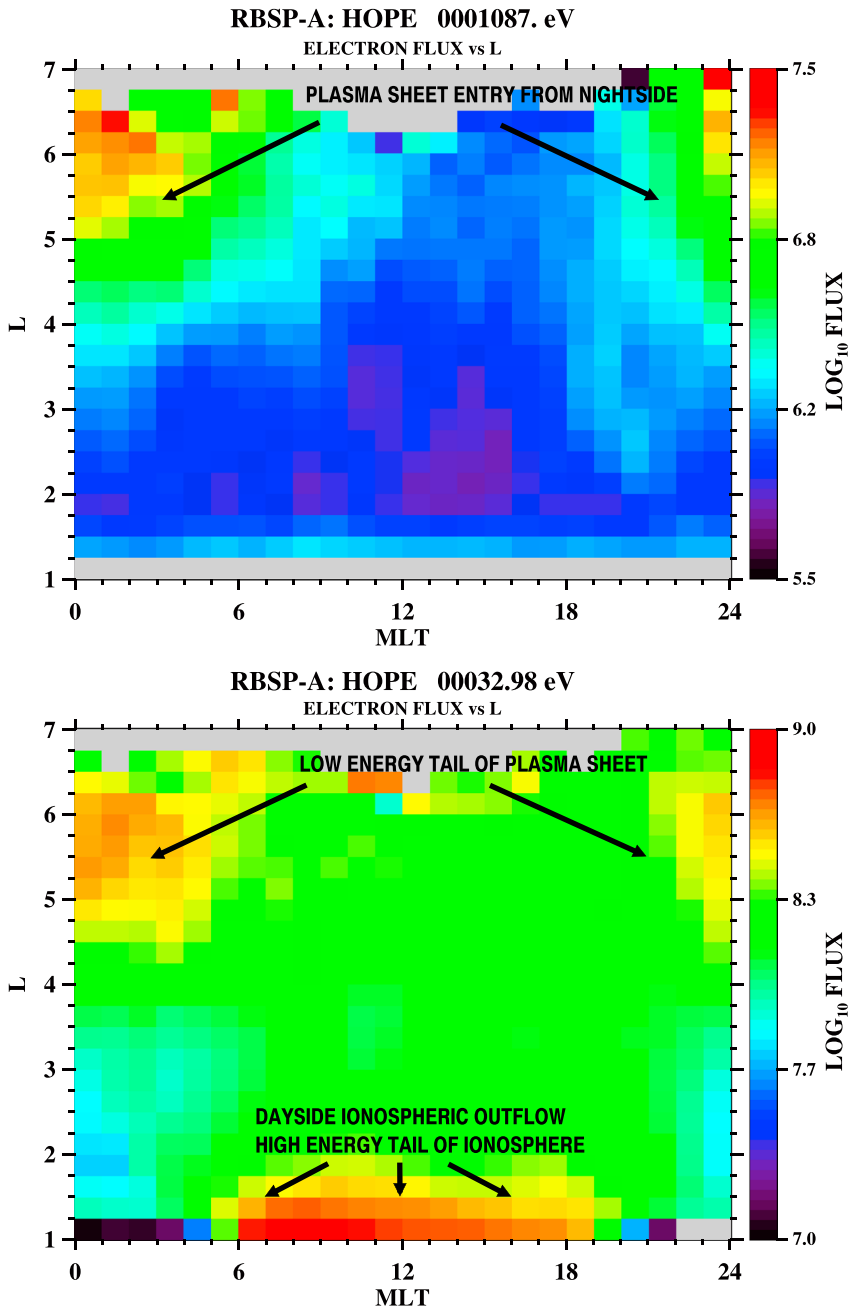

Figure 2. The logarithm of the omnidirectional electron flux ($s^{-1}\,cm^{-2}\,sr^{-1}\,keV^{-1}$) is plotted as a function of magnetic local time (MLT) and L at (top) 32.98 eV and at (bottom) 1087 eV. Each data point measured by HOPE on RBSP-A from 13 October 2012 to 30 May 2016 is plotted, and hence, considerable overlap of points occurs in these plots. Note: at both energies, from L = 1–2, there is evidence of elevated fluxes at all local times. This is more evident ~1 keV where the absolute magnitude of the fluxes is lower.

for the energies under investigation [*Thomsen et al.*, 1999]. Second, over 14 million individual measurements of the flux provide the raw data for each of the plots shown in Figure 3. The mean values thus provide a robust determination of the average spatial variation of the fluxes around GEO (in LT) and the variation of the fluxes with the strength of magnetospheric convection. However, the mean fluxes do neglect temporal variations, which are known to be significant, particularly during disturbed conditions (note: fluxes at GEO at any energy, any local time, and any value of either *Kp* or solar wind electric field can be estimated by the flux models of *Denton et al.* [2015, 2016a]).

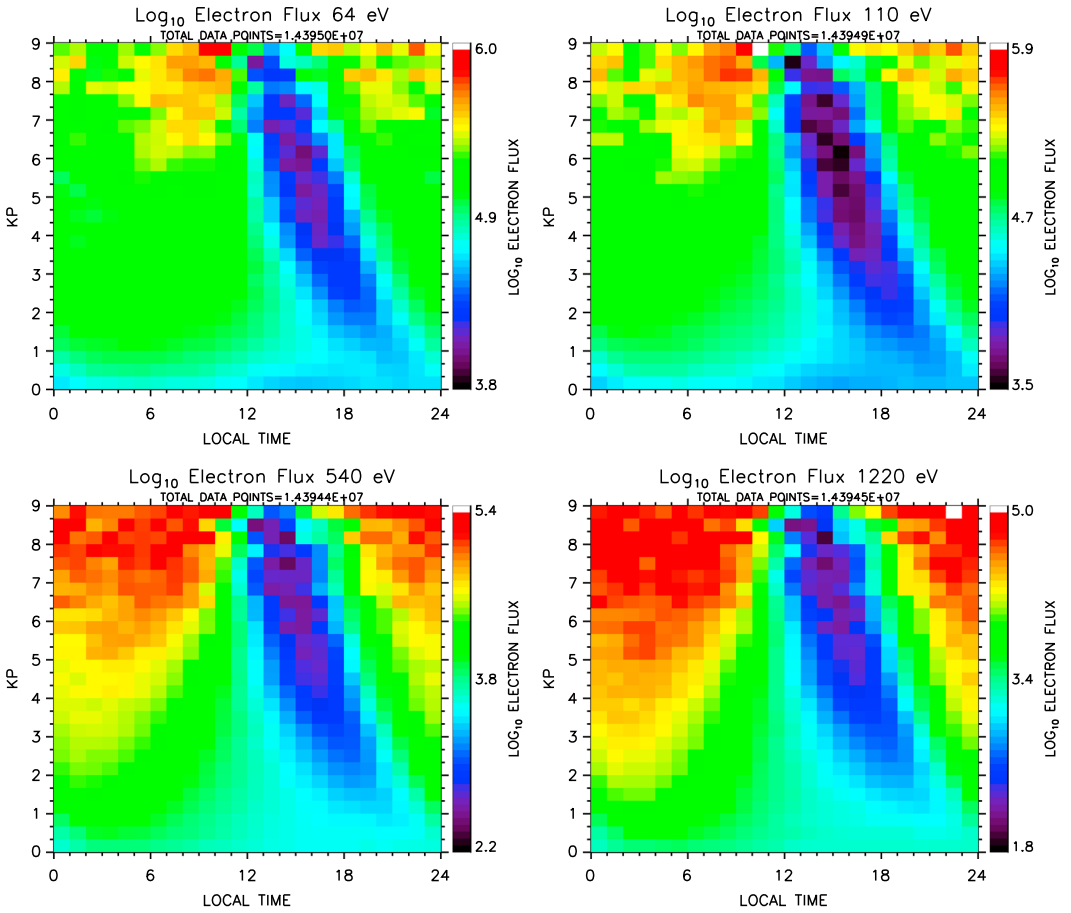

Figure 3. Plots of the averaged omnidirectional flux (s^{-1} cm^{-2} sr^{-1} eV^{-1}) measured by LANL/MPA, as a function of *Kp* and local time, at four energies (~64 eV, ~110 eV, ~540 eV, and ~1220 eV). Intervals where the magnetopause was located inward of GEO or where the spacecraft surface charging level exceeded −40 V are excluded from the analysis.

The plots in Figure 3 demonstrate that, at GEO, the electron population at energies tens of eV, up to typical plasma sheet energies, are very similar in character, since the four plots all have very similar features. Specifically, the fluxes increase with enhanced magnetospheric convection (*Kp* index) and have strong variations with local time. The most prominent feature is the deep minimum in fluxes (at all energies) that occurs in the afternoon sector (for low values of *Kp*) and close to noon (for elevated *Kp* intervals). Previous work has shown that this feature can be explained by consideration of particle drifts through the magnetosphere, and in particular the energy-dependent Alfvén boundaries [*Thomsen et al.*, 1998b; *Korth et al.*, 1999; *Korth and Thomsen*, 2001]. This minimum in electron fluxes corresponds to the region occupied by low-energy (~few eV) ions of the plasmasphere, and at the higher *Kp* values, the plasmaspheric plume [*Denton and Borovsky*, 2008; *Borovsky and Denton*, 2008]. The similar morphology and appearance of the plots in Figure 3 confirm that the fluxes at lower energies (approximately tens of eV) at geosynchronous orbit are dominated by the lower energy tail of the plasma sheet population, with a characteristic energy of a few keV (cf. Figures 1 and 2).

Earthward of geosynchronous orbit, the HOPE observations provide information on the variation in the low-energy electron flux in this region. Figure 4 shows a three-dimensional view of the HOPE omnidirectional electron observations at ~1 keV and ~33 eV, between October 2012 and May 2016, with the flux values projected onto the walls of the plot as a function of MLT, L value, and the *z* component of position in GSM coordinates, in order to reveal the latitudinal spread of the data (left column; note: considerable overlap of points occurs in these plots). The energies of ~33 eV and ~1087 eV are selected as representative of the high-energy tail of the ionospheric population and the plasma sheet population, respectively. The red circle and the red dots in the figure indicate the approximate locations of geosynchronous orbit

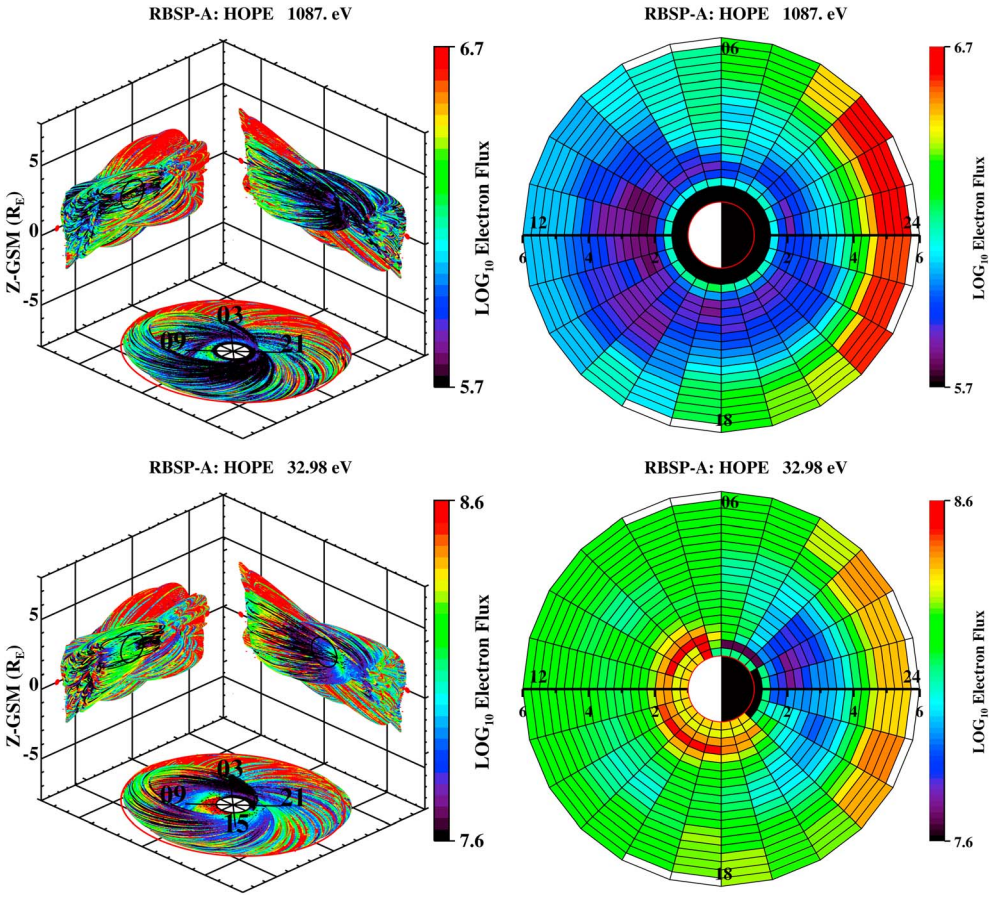

Figure 4. Observations of the omnidirectional electron flux at ~33 eV and ~1087 eV ($s^{-1}\,cm^{-2}\,sr^{-1}\,keV^{-1}$), measured by the HOPE instrument on board Van Allen Probes A between October 2012 and May 2016. (left column) The flux level is denoted by the color and projected onto the walls of the plot as a function of magnetic local time (MLT), L shell, and the *z* component of position in GSM coordinates. Note: considerable overlap of points occurs in the plots in the left column. (right column) The same data binned as a function of MLT and L. It is clear that elevated fluxes occur primarily in two locations: close to the Earth and also in the outer regions of the satellite orbit on the nightside.

at 6.6 Earth radii (R_E). The figure also contains plots of the mean of the same flux data binned as a function of MLT and L value (right column), using a bin size of 1 h in MLT and a bin size of 0.25 in L value (in order to mitigate the overlap of data plotted in the left column).

Studying Figure 4 (and Figure 2), it is clear that the electron fluxes are greatest in two regions. Close to the Earth are high fluxes at ~33 eV across the dayside, which we attribute to outflow from the nearest sunlit ionosphere: an ionospheric source of low-energy electrons. This interpretation is supported by the local times where fluxes are elevated (just after sunrise to just after sunset). At L values between ~2 and 4 there is a minimum in the flux of electrons at this energy that deepens from sunset (~18 MLT) through local midnight, into the postmidnight sector. This local time variation is consistent with a sunlit ionosphere source for electrons at these L values, which is removed during darkness (as the lofted ionospheric supply of plasma to the plasmasphere ceases). At greater distances from the Earth, the electron fluxes at ~33 eV are, in general, elevated on the nightside. These electrons are attributed to the low-energy tail of the plasma sheet population: a plasma sheet source of low-energy electrons.

At ~1 keV, high fluxes of electrons are measured in a ring close to the Earth at all local times, and we interpret this feature as likely contamination from energetic protons. At greater distances from the Earth the electron flux is greatest on the nightside, and this is consistent with expectations of plasma sheet entry into the magnetosphere, with the elevated fluxes centered close to local midnight in local time [cf. *Korth et al.*, 1999; *Denton et al.*, 2005].

To further investigate the electron populations Earthward of geosynchronous orbit, and in particular to attempt to determine the origin of the low-energy electron population, the variation of fluxes as a function of pitch-angle is analyzed. Close to local midnight, upon their entry and arrival into the inner magnetosphere, plasma sheet electrons of a few keV are isotropically distributed in pitch-angle [*Friedel et al.*, 2001; *Denton et al.*, 2005]. As electrons are convected deeper into the magnetosphere, drifting eastward and westward around the Earth, their pitch-angle distribution becomes progressively more anisotropic (peaked at ~90°). This is likely due to the field-aligned component being preferentially lost due to collisions resulting from their deeper penetration into the atmosphere [*Fok et al.*, 1991; *Janev and Smith*, 1993; *Henderson et al.*, 2015; *Denton et al.*, 2016b], although wave-particle interactions (e.g., whistler-mode chorus waves) can also lead to anisotropic distributions. By the time the electrons drift onto the dayside, the distribution becomes strongly peaked around 90°. In contrast, ionospheric-origin electrons that escape from the collisionally dominated atmosphere are preferentially field-aligned, particularly during so-called beam events where the broad distribution of accelerated electrons is typically ~100 s eV [e.g., *Chaston et al.*, 2001]. Hence, the pitch-angle distribution of the electrons provides an excellent tracer to determine the origin of these electrons, whether ionospheric or plasma sheet. Figure 5 shows the electron fluxes (in units of $s^{-1}\,cm^{-2}\,sr^{-1}\,keV^{-1}$) around local midnight (22–02 MLT) and local noon (10–14 MLT) at four energies (~33, 53, 222, 1087 eV) as a function of local pitch-angle and L value. Note: no allowance has been made for latitudinal effects in these data—the aim is to simply reveal a coarse picture of whether the distributions are predominantly field-aligned or perpendicular. Also note that no background subtraction has taken place for this analysis; however, at low energies, the fluxes of the ambient population greatly exceed background levels. At higher energies, the background is concentrated in the region close to the Earth ($<L=2$) (cf. Figure 2).

The plots in Figure 5 show a strong diurnal variation at all energies. At ~33 eV (top row) the highest fluxes around local midnight are found at $L>4$. In this region, the fluxes decrease and the pitch-angle distribution becomes more peaked around 90° in the region between $L=3$ and $L=4$ (the slot region). This picture is consistent with (i) an ionospheric population of low-energy electrons close to Earth, where the field-aligned component is largely absent during hours of darkness, combined with (ii) a plasma sheet source of electrons from the outer magnetosphere, for which the electrons at ~30 eV represent the low-energy tail of the full distribution. In contrast, around local noon, the highest fluxes are observed to occur at lower L values ($L\sim-1$ to 2), and these elevated fluxes are primarily seen at field-aligned pitch-angles. Indeed, elevated fluxes are observed in the field-aligned electrons at all L values around local noon. These observations are consistent with (iii) an ionospheric source of electrons that is field-aligned and that is energized due to the incident solar EUV flux in daylight, combined with (iv) a source of field-aligned electrons at $L>$~6 that are likely present due to energization processes acting upon thermal (ionospheric) electrons at high latitudes. (Note: a complete description of the evolution of the electron energy spectrum during storms in terms of L, for ~keV to ~MeV energies, may be found in recent work also utilizing Van Allen Probes data [*Reeves et al.*, 2013]). At ~50 eV around local midnight, the fluxes are similar to those ~30 eV. However, on the dayside, there is less evidence of a field-aligned population of electrons at high L shells (>~6): the population is more isotropic. This observation adds strength to the conjecture that whatever process is energizing electrons in the high-latitude region, the maximum energization is, on average, ~50–100 eV, consistent with characteristic energies reported in the literature [e.g., *Chaston et al.*, 2001; *Cattell et al.*, 2004; *Teste et al.*, 2007]. The transition between this behavior and that observed at higher energies occurs ~100 eV. At ~200 eV and ~1 keV the highest fluxes are to be found around local midnight at $L>4$, suggesting a strong nightside plasma sheet source of electrons.

Of course the fluxes and pitch-angle distributions shown in Figure 5 represent the average fluxes for all levels of geomagnetic activity. In order to explore the variation of these fluxes with activity, the fluxes are separated into active periods and quiet periods of solar wind driving, based on the value of the solar wind electric field parameter $-v_{sw}B_z$ (in units of $mV\,m^{-1}$). Figure 6 shows the same averaged electron local pitch-angle distributions around local midnight, from Figure 5, but this time separated into quiet and active periods. Figure 6 (left column) shows the electron pitch-angle distributions around local midnight (22–02 MLT) at two energies during quiet periods ($-v_{sw}B_z<-1$), and Figure 6 (right column) shows the fluxes during active periods ($-v_{sw}B_z>1$). This division represents a separation between periods of positive interplanetary magnetic field (IMF) B_z and negative IMF B_z.

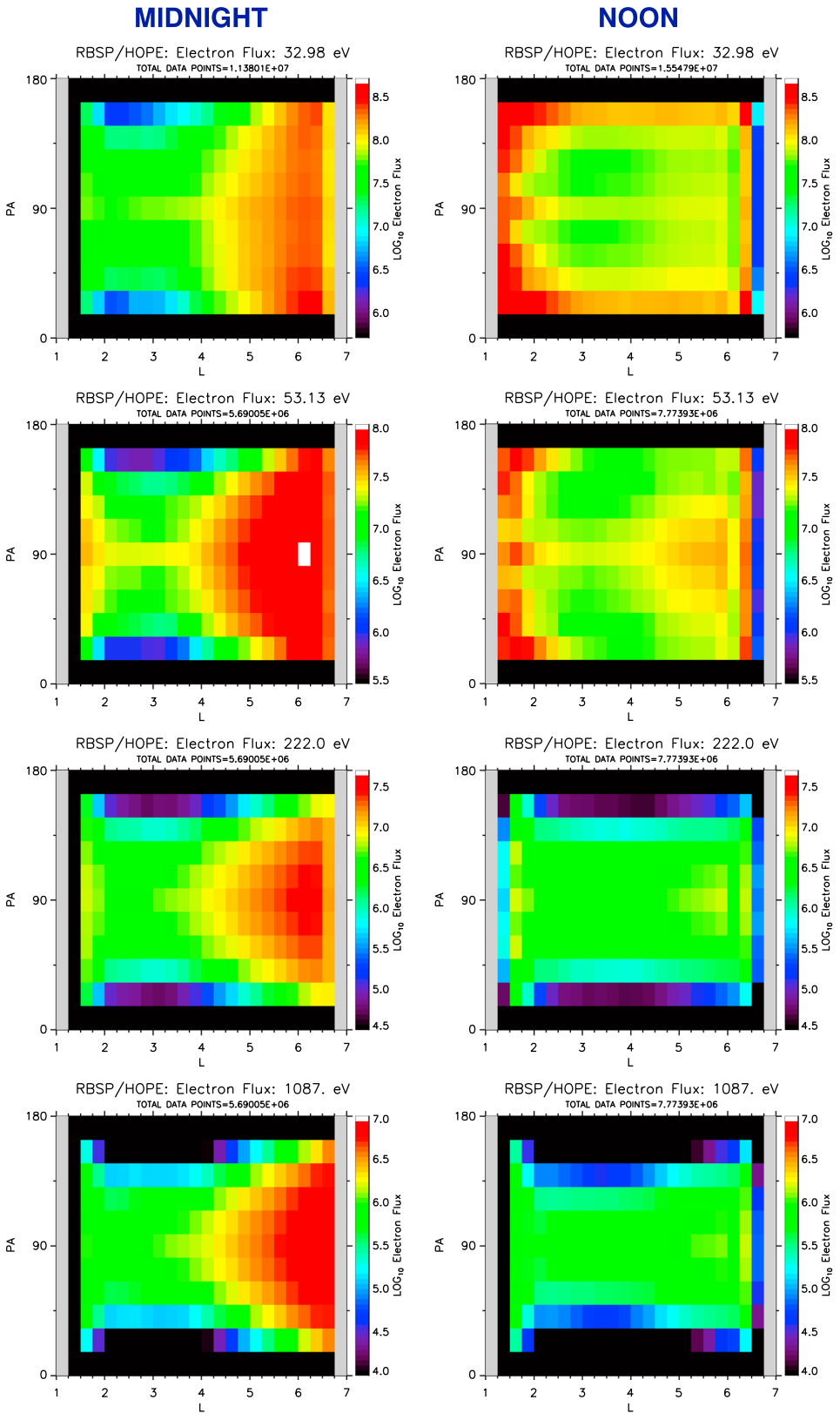

Figure 5. The averaged electron flux ($s^{-1}\,cm^{-2}\,sr^{-1}\,keV^{-1}$) as a function of local pitch-angle and L value around (left column) local midnight (22–02 MLT) and (right column) local noon (10–14 MLT) at four energies.

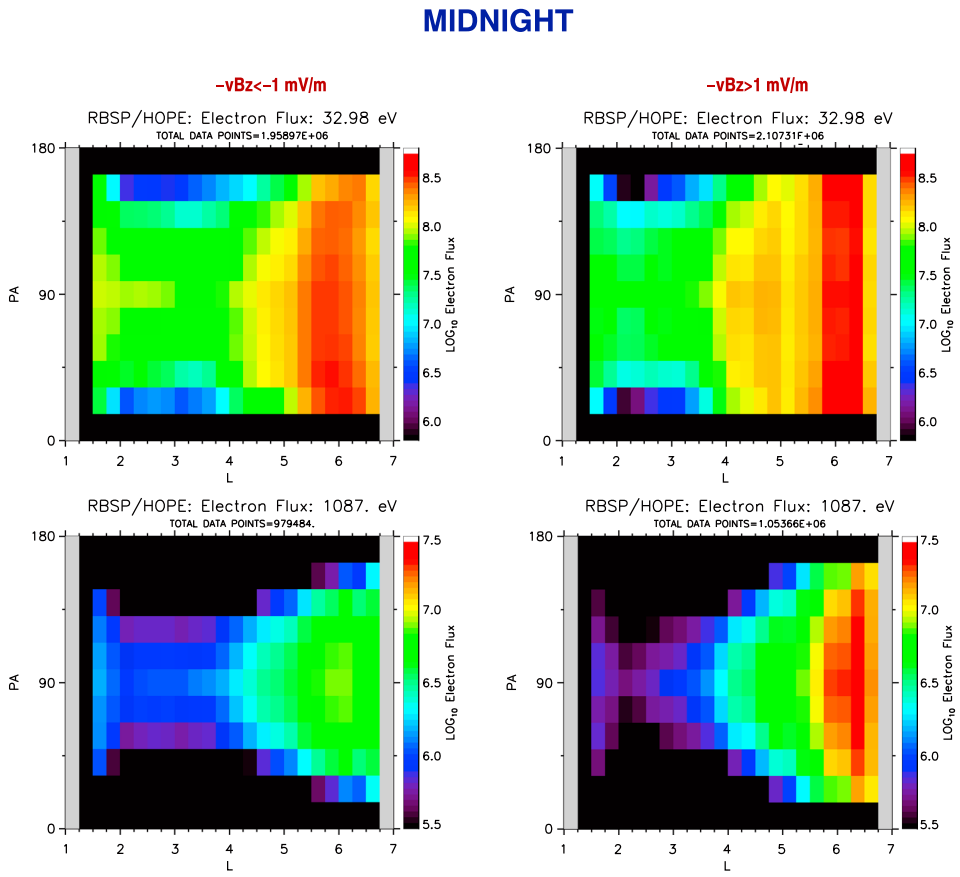

Figure 6. The averaged electron flux ($s^{-1}\,cm^{-2}\,sr^{-1}\,keV^{-1}$) as a function of local pitch-angle and L value around local midnight (22–02 MLT). (left column) Data for low solar wind driving ($-v_{sw}B_z < -1$). (right column) Data for elevated solar wind driving ($-v_{sw}B_z > 1$).

The flux distributions in Figure 6 show significant differences between low solar wind driving (left column) and elevated solar wind driving (right column). During periods of low driving, the electron fluxes at ~33 eV close to Earth are slightly higher at L values less than ~3, when compared to periods of strong solar wind driving. During enhanced geomagnetic activity, a reduced O/N_2 ratio in the thermosphere can reduce the content of the ionosphere and thus lead to a reduced electron flux in the ionosphere/plasmasphere during hours of sunlight and subsequently during darkness [*Prölss*, 1976; *Rishbeth*, 1998]. For L values greater than ~4 the situation is reversed and the fluxes during periods of low-driving are less than during periods of elevated activity. This is consistent with increased convection driving electrons radially inward from the plasma sheet during disturbed periods and supports the interpretation that the elevated nightside electron fluxes at ~33 eV are indeed the low energy tail of freshly delivered plasma sheet material. The isotropic nature of the electrons at $L > 5$ is also consistent with this interpretation [cf. *Denton et al.*, 2005].

At ~1087 eV, during periods of low driving, the electron fluxes are slightly elevated at L values above ~4, when compared to periods of strong solar wind driving. This is again consistent with previous observations that plasma sheet electron convection into the magnetosphere is enhanced during enhanced solar wind driving [cf. results at GEO by *Korth et al.* [1999] and *Denton et al.* [2005]). However, adiabatic effects between quiet times and storm times are also likely to play a role that complicates interpretation of the results.

Figure 7 contains the same sequence of plots as those shown in Figure 6, but this time, for data taken around local noon (10–14 MLT). Here for electrons with energies ~33 eV, the situation is similar to that at local midnight, with much stronger field-aligned fluxes during low solar wind driving compared to high solar wind driving. For electrons with energies ~1087 eV the noon fluxes are again slightly higher during quiet periods than during active periods. This is somewhat surprising given that the electron fluxes around midnight (primarily electrons from the plasma sheet) are actually higher during enhanced solar wind driving.

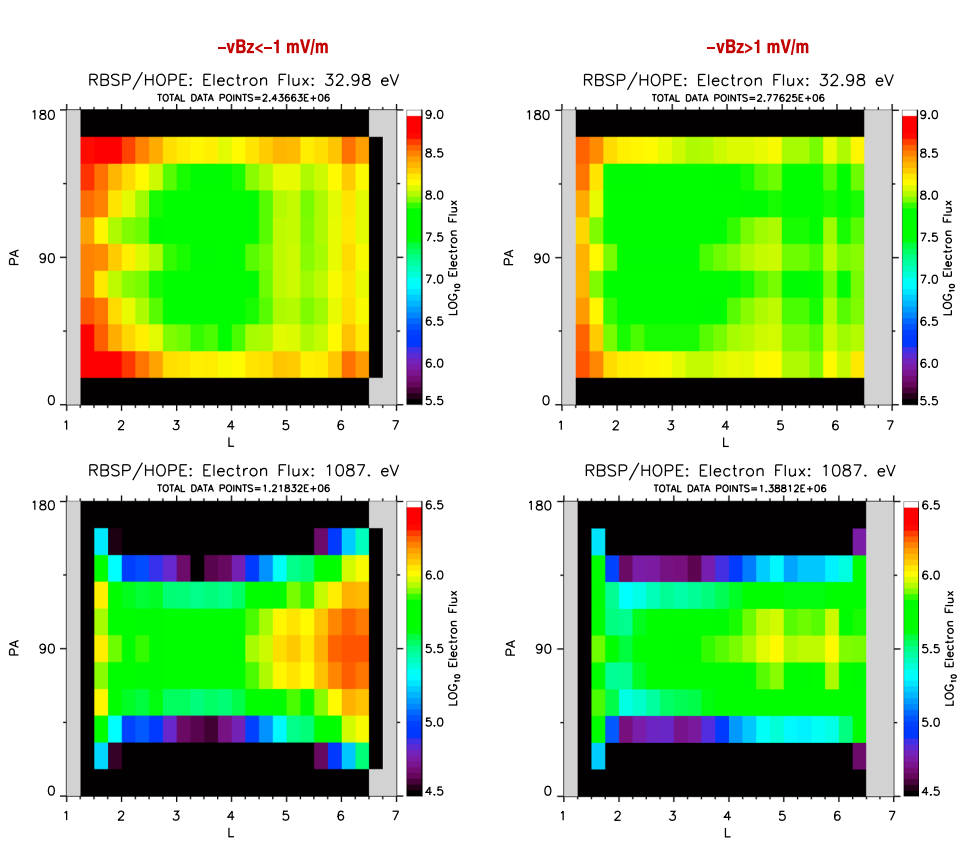

Figure 7. The averaged electron flux ($s^{-1}\,cm^{-2}\,sr^{-1}\,keV^{-1}$) as a function of local pitch-angle and L value around local noon (10–14 MLT). (left column) Data for low solar wind driving ($-v_{sw}B_z < -1$). (right column) Data for elevated solar wind driving ($-v_{sw}B_z > 1$).

However, as electrons drift to the dayside, they are lost primarily via collisions in the atmosphere. During enhanced activity, there will be heating (and expansion) of the neutral atmosphere; meaning, these losses will increase. In addition, the increased convection affects the drift paths taken by electrons of all energies that complicates the interpretation of the results. Furthermore, there are numerous local time-dependent wave-particle processes (e.g., whistler-mode chorus waves) that may modify the distributions and lead to local time asymmetries. A complete study of these processes and their effects on the distributions presented here is beyond the scope of the present study. Case studies of individual storm events using the multisatellite perspective of the Van Allen Probes mission, coupled with theoretical simulations, provide a way to reveal the interconnections between drift physics and in situ energization/loss processes [e.g., *Denton et al.*, 2016b].

4. Conclusions and Summary

The spatial and temporal morphologies of the low-energy electron population have been poorly determined to date. The analysis described here and the results shown in Figures 1 to 7 provide a partial remedy to this. The broad spatial variation of the low-energy electron population and its typical behavior with increasing geomagnetic activity have been determined. In addition, the average pitch-angle distribution of the electrons around noon and midnight, for energies between ~33 eV and ~1087 eV, has been calculated. Evidence from the analysis provides clear confirmation of two source populations for low-energy electrons, namely, the low-energy tail of the electron plasma sheet and the high-energy tail of the outflowing ionosphere.

The flux plots shown in Figure 3 contain broad statistical descriptions of the electron flux at GEO as a function of geomagnetic activity. The highest fluxes, on average, are found at energies between ~60 eV and ~1 keV on

the nightside during the strongest levels of convection (proxied by the *Kp* index). The lowest fluxes, on average, are found in the postnoon sector [cf. *Korth et al.*, 1999; *Denton et al.*, 2005; *Friedel et al.*, 2001]. This is consistent with the plasma sheet being the dominant source at these energies. However, the pitch-angle distributions of the low-energy electrons provide additional information: field-aligned fluxes indicate an ionospheric source, whilst fluxes peaked at ~90° are indicative of a plasma sheet source. The field-aligned distribution of low energy (~33 eV) at all L values (but strongest for L values between 1 and 3 and L values >5) around local noon indicates that the low-energy electron plasma sheet population is supplemented by electrons that are flowing directly out of the dayside ionosphere. The high fluxes at L values $>\sim5$ indicate outflows that are particularly strong from the middle-to-polar ionosphere. From the results shown in Figure 7, it is clear that this outflow occurs during both quiet periods and during active periods.

Concerning the implications of our results for magnetospheric wave-particle interactions, it is well known that low-energy electrons play a vital role in governing the dynamics of whistler-mode waves [*Thorne and Horne*, 1994; *MacDonald et al.*, 2008, 2010]. The distributions of the electrons, in both energy and pitch-angle, along with their MLT and L dependencies, are critical in estimating the effects of such waves, particularly on more energetic (relativistic) particles. We intend that the electron distributions presented here will be proven useful in this regard.

With regard to future work in this area, one possible advance could be made by examining the low-energy electrons and the electrons of plasma sheet energies measured by HOPE, by utilizing a coordinate framework based on the (U, B, K) formulation introduced by *Whipple* [1978]. This formulation, previously used for data at geosynchronous orbit [*Korth et al.*, 1999; *Friedel et al.*, 2001; *Henderson et al.*, 2015], has the advantage of naturally taking account of the particle drift trajectories—and hence would be useful in order to trace the paths of the particles through the system. *Friedel et al.* [2001] examined the access of the plasma sheet to the inner magnetosphere by using POLAR data but restricted their study to pitch-angles of 90° only. Once further data from HOPE have been accumulated, it will be illuminating to carry out a similar study (but with vastly more data) of particle trajectories in the inner magnetosphere, both for electron and ions, for a variety of pitch-angles and energies. This would certainly provide confirmation, or otherwise, for the assertion that suprathermal electrons from the plasma sheet can become trapped at low L shells and go on to form the plasmaspheric electron population [*Li et al.*, 2010]. Recently, *Denton et al.* [2016b] carried out a preliminary examination of O^+ and H^+ ions in the inner magnetosphere during storms and demonstrated that the plasma sheet source at low energies can mimic the local acceleration of the ionospheric source population. A similar future study is planned for the low-energy electrons.

In summary, observations from the HOPE instrument onboard Van Allen Probes B have been used to investigate the sources of low-energy electrons in the inner magnetosphere. We have documented and quantified observed fluxes of this population and calculated the average pitch-angle distributions as a function of L value for both quiet and active periods. It is intended that our results will be proven useful, in combination with future modeling studies, for determining the role of the low-energy electron population in global magnetospheric dynamics. Electrons modulate wave-particle interactions in the magnetosphere, and these interactions govern energy transfer. We intend that the results from this current paper will help to advance the work in this area.

Acknowledgments

The authors gratefully acknowledge the OMNI database for the solar wind and geophysical parameters used in this study. M.H.D. would like to thank Joe Borovsky, Lauren Blum, Jacob Bortnik, Stephen Fuselier, and Lynn Wilson III for helpful discussions. Data from the RBSP-ECT instrument suite used in this study are available at http://www.rbsp-ect.lanl.gov/. LANL/MPA data are available by contacting the instrument principal investigator (mghenderson@lanl.gov). This work was supported at New Mexico Consortium by RBSP Energetic Particle, Composition, and Thermal Plasma funding under NASA's Prime contract NAS5-01072.

References

Bame, S. J., D. J. McComas, M. F. Thomsen, B. L. Barraclough, R. C. Elphic, J. P. Glore, J. C. Chavez, E. P. Evans, and F. J. Wymer (1993), Magnetospheric Plasma Analyzer for spacecraft with constrained resources, *Rev. Sci. Instrum.*, *64*, 1026–1033, doi:10.1063/1.1144173.

Bell, T. F., U. S. Inan, J. Bortnik, and J. D. Scudder (2002), The Landau damping of magnetospherically reflected whistlers within the plasmasphere, *Geophys. Res. Lett.*, *29*(15), 1733, doi:10.1029/2002GL014752.

Bortnik, J., R. M. Thorne, and N. P. Meredith (2007), Modeling the propagation characteristics of chorus using CRRES suprathermal electron fluxes, *J. Geophys. Res.*, *112*, A08204, doi:10.1029/2006JA012237.

Borovsky, J. E., and M. H. Denton (2008), A statistical look at plasmaspheric drainage plumes, *J. Geophys. Res.*, *113*, A09221, doi:10.1029/2007JA012994.

Carpenter, D. L. (1963), Whistler evidence of a "knee" in the magnetospheric ionisation density profile, *J. Geophys. Res.*, *68*, 1675–1682, doi:10.1029/JZ068i006p01675.

Carpenter, D. L., and C. G. Park (1973), On what ionospheric workers should know about the plasmapause-plasmasphere, *Rev. Geophys.*, *11*, 133–154, doi:10.1029/RG011i001p00133.

Cattell, C., J. Dombeck, W. Yusof, C. Carlson, and J. McFadden (2004), FAST observations of the solar illumination dependence of upflowing electron beams in the auroral zone, *J. Geophys. Res.*, *109*, A02209, doi:10.1029/2003JA010075.

Chappell, C. R., K. K. Harris, and G. W. Sharp (1971), OGO 5 measurements of the plasmasphere during observations of stable auroral arcs, *J. Geophys. Res.*, *76*, 2357–2365, doi:10.1029/JA076i010p02357.

Chappell, C. R. (1972), Recent satellite measurements of the morphology and dynamics of the plasmasphere, *Rev. Geophys.*, *10*, 951–979, doi:10.1029/RG010i004p00951.

Chappell, C. R., M. M. Huddleston, T. E. Moore, B. L. Giles, and D. C. Delcourt (2008), Observations of the warm plasma cloak and an explanation of its formation in the magnetosphere, *J. Geophys. Res.*, *113*, A09206, doi:10.1029/2007JA012945.

Chaston, C. C., W. J. Peria, C. W. Carlson, R. E. Ergun, and J. P. McPhadden (2001), FAST observations of inertial Alfvén waves and electron acceleration in the dayside aurora, *Phys. Chem. Earth*, *26*(1–3), 201–205, doi:10.1016/S1464-1917(00)00108-2.

Christon, S. P., D. J. Williams, D. G. Mitchell, C. Y. Huang, and L. A. Frank (1991), Spectral characteristics of plasma sheet ion and electron populations during disturbed geomagnetic conditions, *J. Geophys. Res.*, *96*, 1–22, doi:10.1029/90JA01633.

DeForest, S. E. (1972), Spacecraft charging at synchronous orbit, *J. Geophys. Res.*, *77*, 651–659, doi:10.1029/JA077i004p00651.

Denton, M. H., G. E. Reeves, M. F. Thomsen, M. G. Henderson, R. H. W. Friedel, B. Larsen, R. M. Skoug, H. O. Funsten, H. E. Spence, and C. A. Kletzing (2016b), The complex nature of storm time ion dynamics: Transport and local acceleration, *Geophys. Res. Lett.*, *43*, 10,059–10,067, doi:10.1002/2016GL070878.

Denton, M. H., M. G. Henderson, V. K. Jordanova, M. F. Thomsen, J. E. Borovsky, J. Woodroffe, D. P. Hartley, and D. Pitchford (2016a), An improved empirical model of electron and ion fluxes at geosynchronous orbit based on upstream solar wind conditions, *Space Weather*, *14*, 511–523, doi:10.1002/2016SW001409.

Denton, M. H., M. F. Thomsen, V. K. Jordanova, M. G. Henderson, J. E. Borovsky, J. S. Denton, D. Pitchford, and D. P. Hartley (2015), An empirical model of electron and ion fluxes derived from observations at geosynchronous orbit, *Space Weather*, *13*, 233–249, doi:10.1002/2015SW001168.

Denton, M. H., and J. E. Borovsky (2014), Observations and modeling of magnetic flux tube refilling of the plasmasphere at geosynchronous orbit, *J. Geophys. Res. Space Physics*, *119*, 9246–9255, doi:10.1002/2014JA02049.

Denton, M. H., and J. E. Borovsky (2008), Superposed epoch analysis of high-speed-stream effects at geosynchronous orbit: Hot plasma, cold plasma, and the solar wind, *J. Geophys. Res.*, *113*, A07216, doi:10.1029/2007JA012998.

Denton, M. H., and J. E. Borovsky (2012), Magnetosphere response to high-speed solar-wind streams: A comparison of weak and strong driving and the importance of extended periods of fast solar wind, *J. Geophys. Res.*, *117*, A00L05, doi:10.1029/2011JA017124.

Denton, M. H., M. F. Thomsen, H. Korth, S. Lynch, J. C. Zhang, and M. W. Liemohn (2005), Bulk plasma properties at geosynchronous orbit, *J. Geophys. Res.*, *110*, A07223, doi:10.1029/2004JA010861.

Farthing, W. H., J. P. Brown, and W. C. Bryant (1982), Differential spacecraft charging on the geostationary operational satellites, NASA Tech. Memo, NASA TM-83908.

Fok, M.-C., J. U. Kozyra, A. F. Nagy, and T. E. Cravens (1991), Lifetime of ring current particles due to Coulomb collisions in the plasmasphere, *J. Geophys. Res.*, *96*, 7861–7867, doi:10.1029/90JA02620.

Friedel, R. H. W., H. Korth, M. G. Henderson, M. F. Thomsen, and J. D. Scudder (2001), Plasma sheet access to the inner magnetosphere, *J. Geophys. Res.*, *106*, 5845–5858, doi:10.1029/2000JA003011.

Funsten, H. O., et al. (2013), Helium, Oxygen, Proton, and Electron (HOPE) mass spectrometer for the Radiation Belt Storm Probes mission, *Space Sci. Rev.*, *179*, 423–484, doi:10.1007/s11214-013-9968-7.

Garrett, H. B. (1981), The charging of spacecraft surfaces, *Rev. Geophys.*, *19*, 577–616, doi:10.1029/RG019i004p00577.

Gringauz, K. I., V. V. Bezrukikh, V. D. Ozerov, and R. E. Rybchinskii (1960), Studying the interplanetary ionized gas, energetic electrons, and solar corpuscular radiation using three-electrode traps of charged particles on the second Soviet space rocket, *Dokl. Akad. Nauk SSSR*, *131*, 1302–1304.

Henderson, M. G., J. Woodroffe, V. Jordanova, and C. Harris (2015), Multi-point observations and modeling of particle injections during substorms, Abstract SM13D-2547, presented at 2015 Fall Meeting, AGU, San Francisco, Calif.

Janev, R. K., and J. J. Smith (1993), Cross sections for collisional processes of hydrogen atoms with electrons, protons, and multiply-charged ions, in *Atomic and Plasma Material Interaction Data for Fusion*, vol. 4, pp. 78–79 , IAEA, Vienna.

Johnstone, A. D., and J. D. Winningham (1982), Satellite observations of suprathermal electron bursts, *J. Geophys. Res.*, *87*, 2321–2329, doi:10.1029/JA087iA04p02321.

Kirby, K., et al. (2013), Radiation Belt Storm Probes—Observatory and environments, *Space Sci. Rev.*, *179*, 59–125, doi:10.1007/s11214-012-9949-2.

Klumpar, D. M., and W. J. Heikkila (1982), Electrons in the ionospheric source cone: Evidence for runaway electrons as carriers of downward Birkeland currents, *Geophys. Res. Lett.*, *9*, 873–876, doi:10.1029/GL009i008p00873.

Korth, H., and M. F. Thomsen (2001), Plasma sheet access to geosynchronous orbit: Generalization to numerical field models, *J. Geophys. Res.*, *106*, 29,655–29,667, doi:10.1029/2000JA000373.

Korth, H., M. F. Thomsen, J. E. Borovsky, and D. J. McComas (1999), Plasma sheet access to geosynchronous orbit, *J. Geophys. Res.*, *104*, 25,047–25,061, doi:10.1029/1999JA900292.

Lanzerotti, L. J., C. Breglia, D. W. Maurer, G. K. Johnson III, and C. G. MacLennan (1998), Studies of spacecraft charging on a geosynchronous telecommunications satellite, *Adv. Space Res.*, *22*, 79–82, doi:10.1016/S0273-1177(97)01104-6.

Lavraud, B., M. H. Denton, M. F. Thomsen, J. E. Borovsky, and R. H. W. Friedel (2005), Superposed epoch analysis of dense plasma access to geosynchronous orbit, *Ann. Geophys.*, *23*, 2519–2529, doi:10.5194/angeo-23-2519-2005.

Li, W., R. M. Thorne, J. Bortnik, Y. Nishimura, V. Angelopoulus, L. Chen, J. P. McPhadden, and J. W. Bonnell (2010), Global distribution of suprathermal electrons observed on THEMIS and potential mechanism for access into the plasmasphere, *J. Geophys. Res.*, *115*, A00J10, doi:10.1029/2010JA015687.

MacDonald, E. A., M. H. Denton, M. F. Thomsen, and S. P. Gary (2008), Superposed epoch analysis of a whistler instability criterion at geosynchronous orbit during geomagnetic storms, *J. Atmos. Sol. Terr. Phys.*, *70*, 1789–1796, doi:10.1016/j.jastp.2008.03.021.

MacDonald, E. A., L. W. Blum, S. P. Gary, M. F. Thomsen, and M. H. Denton (2010), High-speed stream driven inferences of global wave distributions at geosynchronous orbit; relevance to radiation belt dynamics, *Proc. Roy. Soc. A.*, *466*, 3351–3362, doi:10.1098/rspa.2010.0076.

Mauk, B. H., N. J. Fox, S. G. Kanekal, R. L. Kessel, D. G. Sibeck, and A. Ukhorskiy (2013), Science objectives and rationale for the Radiation Belt Storm Probes mission, *Space Sci. Rev.*, *179*, 3–27, doi:10.1007/s11214-012-9908-y.

Olsen, R. C. (1982), The hidden ion population of the magnetosphere, *J. Geophys. Res.*, *87*, 3481–3488, doi:10.1029/JA087iA05p03481.

Olsen, R. C., C. R. Chappell, D. L. Gallagher, J. L. Green, and D. A. Gurnett (1985), The hidden ion population—Revisited, *J. Geophys. Res.*, *90*, 12,121–12,132, doi:10.1029/JA090iA12p12121.

Prölss, G. W. (1976), On explaining the negative phase of ionospheric storms, *Planet. Space Sci.*, *24*, 607–609, doi:10.1016/0032-0633(76)90140-9.

Reeves, G. D., et al. (2016), Energy-dependent dynamics of keV to MeV electrons in the inner zone, outer zone, and slot regions, *J. Geophys. Res. Space Physics*, *121*, 397–412, doi:10.1002/2015JA021569.

Rishbeth, H. (1998), How the thermospheric circulation affects the ionospheric F2-layer, *J. Atmos. Sol. Terr. Phys.*, *60*, 1385–1402, doi:10.1016/S1364-6826(98)00062-5.

Sarno-Smith, L. K., M. W. Liemohn, R. M. Katus, R. M. Skoug, B. A. Larsen, M. F. Thomsen, J. R. Wygant, and M. B. Moldwin (2015), Postmidnight depletion of the high-energy tail of the quiet plasmasphere, *J. Geophys. Res. Space Physics*, *120*, 1646–1660, doi:10.1002/2014JA020682.

Sarno-Smith, L. K., B. A. Larsen, R. M. Skoug, M. W. Liemohn, A. Breneman, J. R. Wygant, and M. F. Thomsen (2016), Spacecraft surface charging within geosynchronous orbit observed by the Van Allen Probes, *Space Weather*, *14*, 151–164, doi:10.1002/2015SW001345.

Spence, H. E., et al. (2013), Science goals and overview of the Radiation Belt Storm Probes (RBSP) Energetic Particle, Composition, and Thermal Plasma (ECT) Suite on NASA's Van Allen Probes mission, *Space Sci. Rev.*, *179*, 311–336, doi:10.1007/s11214-013-0007-5.

Storey, L. R. (1953), An investigation of whistling atmospherics, *Phil. Trans. Roy Soc. (London), Ser. A*, *246*, 113–141, doi:10.1098/rsta.1953.0011.

Teste, A., D. Fontaine, J.-A. Savaud, R. Maggiolo, P. Canu, and A. Fazakerley (2007), CLUSTER observations of electron outflowing beams carrying downward currents above the polar cap by northward IMF, *Ann. Geophys.*, *25*, 953–969, doi:10.5194/angeo-25-953-2007.

Thomsen, M. F., M. G. Henderson, and V. K. Jordanova (2013), Statistical properties of the surface-charging environment at geosynchronous orbit, *Space Weather*, *11*, 237–244, doi:10.1002/swe.20049.

Thomsen, M. F. (2004), Why *Kp* is such a good measure of magnetospheric convection, *Space Weather*, *2*, S11004, doi:10.1029/2004SW000089.

Thomsen, M. F., M. H. Denton, B. Lavraud, and M. Bodeau (2007), Statistics of plasma fluxes at geosynchronous orbit over more than a full solar cycle, *Space Weather*, *5*, S03004, doi:10.1029/2006SW000257.

Thomsen, M. F., J. E. Borovsky, D. J. McComas, and M. R. Collier (1998a), Variability of the ring current source population, *Geophys. Res. Lett.*, *25*, 3481–3484, doi:10.1029/98GL02633.

Thomsen, M. F., D. J. McComas, J. E. Borovsky, and R. C. Elphic (1998b), The magnetospheric trough, in *Encounter Between Global Observations and Models in the ISTP Era*, *Geophys. Monogr. Ser.*, vol. 104, edited by J. L. Horwitz, D. L. Gallagher, and W. K. Peterson, pp. 355–369, AGU, Washington, D. C.

Thomsen, M. F., E. Noveroske, J. E. Borovsky, and D. J. McComas (1999), Calculation of moments from measurements by the Los Alamos Magnetospheric Plasma Analyzer, Los Alamos Natl. Lab. Rep., LA-13566-MS.

Thorne, R. M., and R. B. Horne (1994), Landau damping of magnetospherically reflected whistlers, *J. Geophys. Res.*, *99*, 17,249–17,258, doi:10.1029/94JA01006.

Whipple, E. C. (1978), (U, B, K) coordinates: A natural system for studying magnetospheric convection, *J. Geophys. Res.*, *83*, 4318–4326, doi:10.1029/JA083iA09p04318.

Wygant, J., et al. (2013), The electric field and wave instruments on the Radiation Belt Storm Probes mission, *Space Sci. Rev.*, *179*, 183–220, doi:10.1007/s11214-013-0013-7.

Zwolakowska, D., P. Koperski, and B. Popielawska (1992), Plasma populations in the tail during northward IMF, Proceedings of the 1st International Conference on Substorms, ESA SP-335, pp. 57–62.